Research Article

Mahboob Alam*

Photocatalytic activity of biogenic zinc oxide nanoparticles: *In vitro* antimicrobial, biocompatibility, and molecular docking studies

https://doi.org/10.1515/ntrev-2021-0069
received May 31, 2021; accepted August 14, 2021

Abstract: The biogenic synthesis of zinc oxide nanoparticles (ZnO NPs) with pinecone extract (PCE) as a reducing agent and antibacterial agent was explored. The current study aims to investigate the biosynthesis of ZnO NPs and their effect on photocatalytic dye degradation and antimicrobial properties. The physical, chemical, and morphological properties of biogenic ZnO NPs synthesized using PCE were investigated using advanced spectroscopy techniques such as Fourier transform infrared spectroscopy (FTIR), UV-visible spectroscopy, transmission electron microscopy (TEM) analysis, selected area electron diffraction (SAED), and X-ray diffraction (XRD) techniques. The photocatalytic degradation of methylene blue was measured spectrophotometrically using biogenic ZnO NPs as nanocatalysts, and decolonization of solution indicates dye degradation gradually as exposure duration increases. The antimicrobial properties of ZnONPs against the tested pathogenic strains were demonstrated using the disc diffusion method. The antimicrobial efficacy of ZnONPs was further explained using molecular docking analysis. Confirmation of the lowest binding energy was used to predict receptor binding site with NPs in order to understand the mechanistic approach. ZnONPs are likely to interact with pathogens *via* mechanical enfolding, which could be one of the major toxicity actions of ZnONPs against strains. Furthermore, the nontoxicity and biocompatibility of ZnO NPs were studied, revealing impressive hemocompatibility with red blood cells (RBCs) and no significant toxicity to Brine shrimps at lower ZnONP concentrations.

Keywords: biogenic synthesis, pinecone extract, photocatalytic degradation, antimicrobial activity, docking

1 Introduction

Nanoparticles are thought to be the basic building blocks of nanotechnology. The highest surface-to-volume ratio of nanoparticles (NP) is the most important and distinguishing feature [1,2]. Nanotechnology now makes a significant contribution to the betterment of human life and has emerged as a multidisciplinary research field. Green nanotechnology, one of the many fields of nanotechnology, provides more effective nanoparticle synthesis with predictable results at a lower cost. Because of their unique properties and benefits in agriculture and other fields, nanomaterials (NPs) have received a lot of attention in recent years. Global production of NP is estimated to be 260,000–309,000 metric tons [3], with global consumption of nanomaterials ranging from 225,060 metric tons to 585,000 metric tons from 2014 to 2019 (2014) [4]. It has been demonstrated that nanomaterials absorb 15–20 times more than bulk particles [5]. ZnO NP levels in the environment ranged from 3.1–31 g/kg in soil to 76–760 g/L in water [6]. Zinc oxide nanoparticles (ZnO NPs) have the potential to improve crop yield and agricultural production [7]. Nanomaterials have sparked interest in the treatment of plant diseases caused by a variety of plant pathogens [8]. Antimicrobial properties of several metals and their ions have been used in various ways since ancient times, for example, utensils made of Cu, Ag, copper with zinc added (brass), and bronze were used in ancient Persia, Rome, and Egypt [9]. Antimicrobial activity has been found in a wide range of metals, including Ag, Al, As, Cd, Co, Cr, Cu, Fe, Ga, Hg, Mo, Mn, Ni, Pb, Sb, Te, and Zn [10–12]. Antimicrobial activity associated with metal ions is based on their capacity to inhibit enzymes, facilitate the production of reactive oxygen species (the Fenton reaction), damage cell membranes, and hinder microorganisms from absorbing essential microelements. Furthermore, several metals and their oxides have genotoxic properties [13–20]. Therefore. ZnO NPs also have the potential to be an effective antibacterial agent against

* **Corresponding author: Mahboob Alam,** Division of Chemistry and Biotechnology, Dongguk University, 123, Dongdae-ro, Gyeongju-si 780-714, Republic of Korea, e-mail: mahboobchem@gmail.com

microorganisms [7]. The environmentally friendly green mediated synthesis of inorganic NP, which includes synthesis through plants, algae, bacteria, fungi, and biological approaches with limited use of expensive and toxic chemicals, is a rapidly expanding area of research in nanotechnology [21]. Concerns about the safety, biocompatibility, and toxicity of nanomaterials, on the other hand, have arisen as their application in a wide range of research and technology fields has grown. The biocompatibility of NP is obviously critical for any therapeutic application. Assessing their potential cytotoxicity, either because of their shape (*e.g.*, needle-like carbon nanotubes), chemical composition (*e.g.*, heavy metals), properties (*e.g.*, carbon nanotubes that have reached the lungs are significantly more toxic than carbon black and graphite), or the interaction of the nanoparticle surface with the cells, is a key issue in evaluating their biocompatibility [22–27]. Therefore, there is an urgent need to address these concerns and improve our understanding of nanomaterials' safety, biocompatibility, and toxicity and to consider the possibility of growing interactions between nanomaterials and biological systems [28–30]. The plant extract-based biosynthesis method has gained popularity as a simple and viable alternative to traditional chemical and physical methods. Green synthesis of ZnO NPs from various plant materials and their potential applications in biology have previously been reported [31,32]. ZnONPs have piqued the interest of researchers due to their wide range of applications in photography, catalysis, biosensors, biomolecular detection, diagnostics, and particularly antimicrobial activity, antimicrobial paint coatings, water treatment, textiles, medical devices, and HIV prevention and therapy [33–42]. Pine cone extract obtained from *Pinus densiflora* (Korean red pine) is antiviral, antimicrobial, antiparasitic, antitumor, and a potent antioxidant [43]. It also helps to boost the immune system. Pine cone extract is thought to have various health benefits, including preventing the growth of HIV in human T cells, the growth of influenza, the growth of the herpes simplex virus, tumor activity, suppressing lymphoma malignancy that involves immune system cells, and boosting the immune system [44–48]. Terpenes, phenolic compounds, cinnamic acid, caffeic acid, chlorophyll components, inorganic and organic components, vitamins, and other chemical substances found in aqueous extract of pine cone from *Pinus densiflora* (Korean red pine) [44,49] can reduce Zn ions to Zn and operate as a topping and balancing specialist [50]. In this study, ZnONPs were green produced using pine cone extract (PCE) and microwave irritation to shorten nanoparticle manufacture time. Biosynthesized ZnONPs were characterized by various techniques. ZnONPs were tested *in vitro* for antimicrobial activity against Gram-positive bacteria, Gram-negative bacteria, and fungi. In addition, this study demonstrated that ZnO NPs are a promising, extraordinarily efficient, and stable photocatalyst for degrading organic dye molecules at room temperature with visible light illumination. Furthermore, due to their environmentally friendly manufacture, the nontoxicity and biocompatibility of ZnO NPs were examined as viable choices for biomedical and environmental applications.

2 Materials and methods

2.1 Pine cone extraction procedure

Pine cones of *Pinus densiflora* belonging to Pinaceae family, a popular tree in Korea, were collected at Dongguk University in Gyeoengju, Republic of Korea. Two pinecones were properly cleansed with distilled water to remove any tainted contents and air dried in the sunlight before being sliced into small pieces and placed in a flask with 100 mL nanopure water and 25 mL ethanol and refluxed for 2 h to obtain the extract. For further processing, pine cone extracts (PNE) were cooled to room temperature and filtered through Whatman filter paper No. 1.

2.2 Biosynthesis of ZnONPs

A precursor was made by adding 10 mL of pine cone extract to 50 mL of 0.1 M zinc acetate ($Zn(CH_3COO)_2H_2O$, Aldrich) aqueous solution in an Erlenmeyer flask at room temperature with gentle stirring. 25 mL of NaOH (aq.) (2 M) solution was gradually added to the solution under stirring to maintain pH in the 10–12 range to attain smaller size particles [51]. In the precursor solution, a PCE extract was added to act as a reducing and capping agent. Following that, the mixed solution was microwaved at a steady power of 800 W for 180 s, or the solution was placed on a magnetic stirrer at 60°C for 6 h. The yellowish-brown tint of the solution indicated particle production. The resultant solution was centrifuged at 10,000 rpm for 10 min, and the unreacted portion of the solution was removed by washing with deionized water 4–5 times and ethanol 3 times to eliminate organic contaminants. After washing, the sample was dried in a 50°C oven. In UV-visible spectroscopy, a peak in the range of 377 nm was found, indicating the reduction of Zn^{2+} to Zn^{0} as well as confirmation of the formation of ZnO NPs.

2.3 Characterizations of ZnO NPs

After the color shift, the reduced ZnO NPs produced by PCE were scanned using a UV-Vis spectrophotometer (UV-1800-Shimadzu) with a dual beam operating at 1 nm resolution within a working wavelength range of 200–700 nm. The X-ray diffraction (XRD) technique was used to investigate the crystallographic characteristics of ZnO NPs within 2θ = 10–80 utilizing the XRD apparatus (Rigaku, Japan) with a Copper Line Focus X-ray tube producing Kα radiation (Cu LFF = 1.540598 Å) as a radiation source. The size of the biogenic ZnO NPS particles was calculated using the Debye–Scherrer equation ($D = K\lambda/(\beta \cos\theta)$; where D is the size of crystalline, λ is the X-ray wavelength, β is the full line width at the half maximum (FWHM), and θ is the Bragg's angle. Transmission electron microscopy (Hitachi, TEM) and selected area electron diffraction (SAED) were used to analyze the morphology features of a sample of bioproduced ZnONPs, including the purity, size, shape, and polydispersity. Fourier transform infrared spectrometry (FTIR) was used to identify functional groups in the extract that could be responsible for the reduction of Zn ions to Zn using KBr pellet in the 500–4,000 cm^{-1} range.

2.4 Photocatalytic degradation

The photocatalytic degradation properties of biogenic ZnO NP were examined using methylene blue (10 mg/L) in aqueous solution under direct sunlight irradiation [52–54]. The calculated quantity (50 mg) of ZnO NPs and dye were poured in water and kept to constant stirring in the dark for an hour to achieve equilibrium. After that, the solution mixture was exposed to direct sunlight for 80 min. Approximately 2 mL of suspension was withdrawn at selected intervals (0, 10, 20, 40, and 80 min) and then catalyst was separated by centrifugation, and the remaining dye concentration was determined by recording UV absorption spectra to measure the degradation of the dye solution at 664 nm. The following equation was used to calculate photocatalytic degradation efficiency. % Degradation = $A_0 - A/A_0 \times 100\%$; where A_0 and A are the initial and final dye solution absorbances at time interval, respectively. To determine the absorption loss, the control experiments were performed in the dark.

2.5 Antimicrobial assay

Using a disc diffusion assay [55,56], the antimicrobial potential of the extracts (PCE) and its biosynthesized ZnONPs were assessed against two bacteria strains, *Escherichia coli* (Gram-negative) and *Bacillus subtilis* (Gram-positive), as well as two human pathogenic fungi; *Humicola insolens* and *Mucor indicus*. Both bacterial strains were cultured in LB broth at 37°C for 24 h on LB agar plates to obtain the bacterial suspensions. However, fungi were cultured on potato dextrose agar at 25°C in the dark. A sterilized glass spreader was used to disperse the strains suspensions (1×10^6) on LB/PD agar plates. Sterile filter paper discs (6 mm diameter) were loaded with fixed concentrations of ZnO NPs, with negative control (sterile water) and positive control (standard antibiotic; Cefepime for bacteria and Clotrimazol for fungi). Following that, all plates were incubated at 37°C. (24 h). After incubation, the inhibitory zone produced by different nanoparticle concentrations was calculated. All tests were carried out in triplicate.

2.6 *In vitro* biocompatibility and cytotoxicity effects on brine shrimps (*Artemia salina*)

Fresh human red blood cells (RBCs) were used to demonstrate biocompatibility in the hemolytic assay, which was carried out according to a previously established methodology with some modification [57–59]. In brief, 1 mL of human whole blood was placed in a tube containing 10% EDTA as an anticoagulant and centrifuged at 500 g for 10 min to discard the serum. After centrifugation, the supernatant and pellet were separated; the supernatant as a serum was discarded. The RBCs as pellets were then resuspended in 5 mL of phosphate buffered saline (PBS) and washed several times by centrifugation (3,000*g*, 3 min each time). PBS–erythrocyte suspension is made by combining 200 µL of RBCs with 9.8 mL of PBS. The erythrocyte suspensions and different concentration of biogenic ZnO NPs (400, 200, 100, 50, and 25 µg/mL) were then combined in Eppendorf tubes. The erythrocyte suspension and biogenic NPs were incubated in Eppendorf tubes for 1 h at 35°C with continuous stirring at 150 rpm, followed by centrifugation at 1,377*g* for 10 min at room temperature. The supernatant obtained by centrifugation was transferred to a 96-well plate and absorbance at 570 nm was recorded. The positive control was 0.5% Triton X-100, while the negative control was PBS and sterile water. The percentage of hemolysis was calculated using the formula below.

$$\% \text{ Hemolysis} = (A - \text{NCA})/(\text{PCA} - \text{NCA}) \times 100$$

where A, NCA, and PCA are the absorbances of the sample, negative control, and positive control, respectively.

The cytotoxicity of ZnONPs to brine shrimp (*Artemia salina*) was tested according to the protocol described [60–62]. One of the key advantages of employing Artemia as a bioassay organism over other zooplankters is that it does not require any maintenance or stock rearing. Brine shrimps with body lengths ranging from 0.8 to 1.0 cm were chosen after hatching saline eggs in 35 g in mL artificial saltwater in a tray near a light source at 37°C. At this point, test samples (12.5–400 µg/mL) were loaded into each well, and the adjusted volume was 0.5 mL. The control solution was 5% salty water without NPs. Throughout the experiments, the temperature was kept at around 27–28°C. Experiment wells with varied concentrations and 10 brine shrimps were left for 24 h. After exposing brine shrimps to NPs solution for 24 h, the number of dead brine shrimps with no visible movement was examined and counted using a magnifying lens. The experiment was carried out in triplicate.

2.7 Molecular docking

A molecular docking study was conducted using the AutoDock method [63] to determine the preferred binding mode and binding sites in complex of ZnONPs and protein receptor. The 3D synthesis of beta-ketoacyl-acyl carrier protein synthase III (FabH) (PDB: 1HNJ), extracted from the RCSB Protein Data Bank, plays a significant role in bacterial to fatty acid bioavailability. The ZnO crystallographic information file (CIF) was obtained from the materials project website. The retrieved CIF of ZnO was saved in PDB format and used as a ligand for docking research. Prior to the simulation study, the ZnO NPs and receptor were subjected to Gasteiger partial charges, Kolman charges, polar hydrogen atoms, and the Lamarckian genetic algorithm. In this docking study, the autogrid was tweaked to produce a large grid map covering the entire surface of the protein. The pose that claimed the highest negative binding energy was considered the best docked model that was further used to visualize binding sites using the BIOVIA software [64].

3 Results and discussion

Pinecone extract (PCE) was used to produce ZnO NP biogenically from aqueous zinc acetate solution. Initially, the PCE and zinc acetate solution reaction mixture gradually changes to the yellow-brown color of the solution. The GC-MS findings for the phytochemical analysis of the aqueous extraction of various part of *Pinus densiflora* including pine cones were previously published [43,65] and revealed the presence of α-pinene, β-pinene, camphene, polyphenols, flavonoids, β-phellandrene, including inorganic and organic components, and vitamins. Polyphenols and flavonoids, for example, play an important role in the biogenic synthesis of NP by reducing ions and stabilizing NP. These biomolecules have the unusual property of attaching to metal surfaces and forming a coat over ZnONPs to shield them from the aggregation process. As shown in the scheme, a tentative mechanism for the biosynthesized NP can be given based on the bioactive presence, especially phenolic, and its involvement in the reduction of Zn^{2+} ions to Zn particles (Scheme 1).

3.1 UV-Vis spectroscopy analysis

The formation of biogenic ZnONPs was confirmed using UV-Visible spectrum that detected well-defined exciton band at 377 nm as shown in Figure 1, which is of the same nature as previously reported [66]. This value is very similar to the bulk exciton absorption of ZnO (373 nm). As a result, the appearance of a single peak at around 377 nm suggests the formation of distorted spherical ZnO NPs with an average size of 40–60 nm. The finding shows that excitation of a nanoparticle from its ground state to its excited state increases absorbance value rapidly. There was a decline in radiation absorption, which may be attributed to agglomeration of prepared NP. The bandgap energy (E_g) was measured and revealed to be 3.29 eV, indicating that ZnONPs might have excellent optical properties.

3.2 XRD analysis

The peculiar peaks pattern of PXRD graphs confirmed and validated the biogenic ZnO NP synthesized utilizing

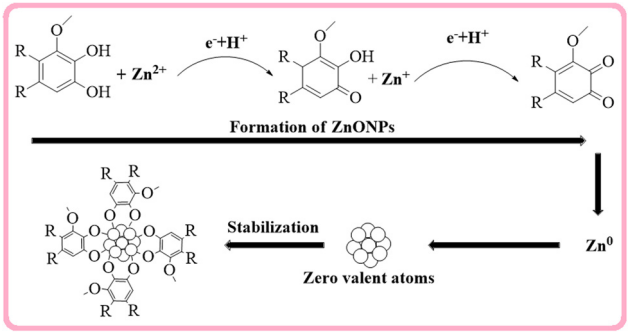

Scheme 1: Tentative mechanism for biogenic synthesis of ZnO NPs using PCE.

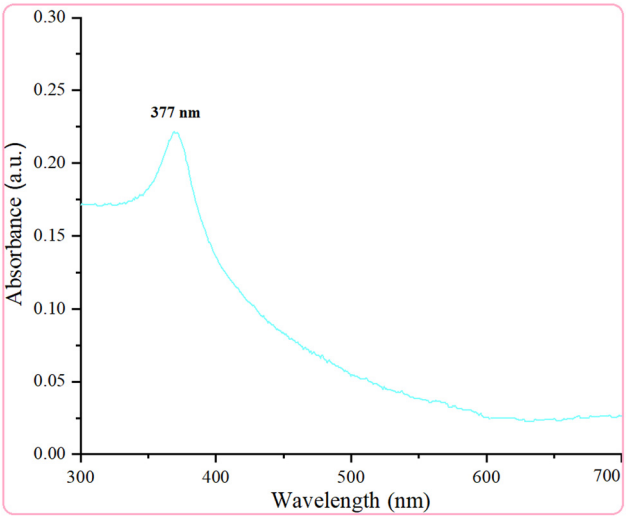

Figure 1: UV-Vis absorption spectra of ZnONPs.

PCE as demonstrated in Figure 2. It shows prominent diffraction peaks indexed on lattice planes 100, 002, 101, 102, 110, 103, and 112° at 2θ values of 31.31, 34.35, 36.21, 47.31, 56.51, 62.70, and 66.25, respectively. These peaks are related to the spherical and hexagonal wurtzite structural phases of zinc oxide, which are listed in JCPDS cards (No. 36-1451, 87-0720, 89-7102, and reference code 01-079-0206). Similar patterns of peaks for the ZnONPs have been also reported [67,68]. The distinct diffraction peaks demonstrate a well-crystallized structure of biogenic ZnONP, which is supported by the strong and narrow peak shape in PXRD pattern. The unassigned peaks were thought to be originated by bioorganic phases that appeared as a notch on the well-visible peaks of the NP. The mean particle sizes of the ZnONPs were calculated from the full width at half maximum (FWHM) using Scherrer's equation as given in literature and found to be about 18.98 nm; however, the larger particle size determined by HRTEM suggested a single nanoparticle encapsulating numerous nanocrystallites.

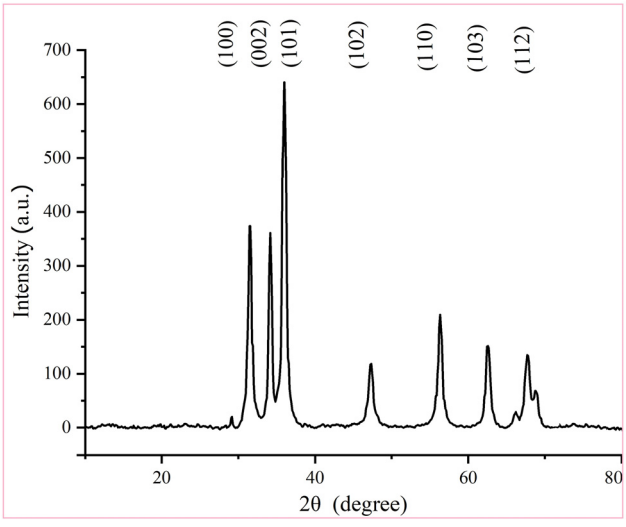

Figure 2: XRD pattern of the biogenic ZnONPs.

3.3 FTIR analysis

The FTIR of biosynthesized ZnONPs was utilized to confirm putative functional groups of extracts and to involve potential bioactive compounds for reduction of Zn^{2+} to Zn^{0} and capping and stability of bio-reduced ZnO NPs manufactured using extract. As can be seen from Figure 3 of IR spectrum, a broad peak at 3,371 cm^{-1} could be assigned markedly to O–H stretching vibration [66] of the alcohol functionality, whereas a broad peak with low strength in the IR spectrum of ZnONPs compared to the FTIR of extract was found to be around 3,400 cm^{-1}, indicating the participation of bioactive compounds with OH groups in the formation of ZnONPs. Other informative peaks were found at 2,890 and a slightly split peak at 1,639 cm^{-1} that can be attributed to C–H, and C═C fused with C═O, stretching vibration of alkane groups and ketones, respectively. The prominent peak about 499 cm^{-1} in FTIR spectrum of ZnONPs matching to metal–oxygen (M–O) supports the formation of NP [69]. Spectral analyses of the extract revealed that phytochemicals such as phenol, terpenes, and flavonoids may play an active role in the reduction of metal ions to metal.

3.4 High-resolution transmission electron microscopy and SAED pattern of ZnONPs

Transmission electron microscopy was used to examine the morphology and structure of biogenically synthesized ZnO NPs in depth. The Figure 4 depicts the transmission electron microscopy image (a), high-resolution transmission electron microscopy image (b), and SAED pattern (c) of ZnO NP synthesized using the green channel and biogenic. The particle size of synthesized ZnO NPs is around 40–60 nm and has a sphere-like morphology. The SAED pattern of as-synthesized ZnO NPs reveals the crystalline structure, and planes are also indicated in the SAED images. The peaks shown by the ZnO NP PXRD pattern can also be seen in the SAED analysis from the core, *i.e.*, 100, 101, 110, and 103, which contains the majority of spherical crystalline ZnONPs. The SAED results agree well with the PXRD results.

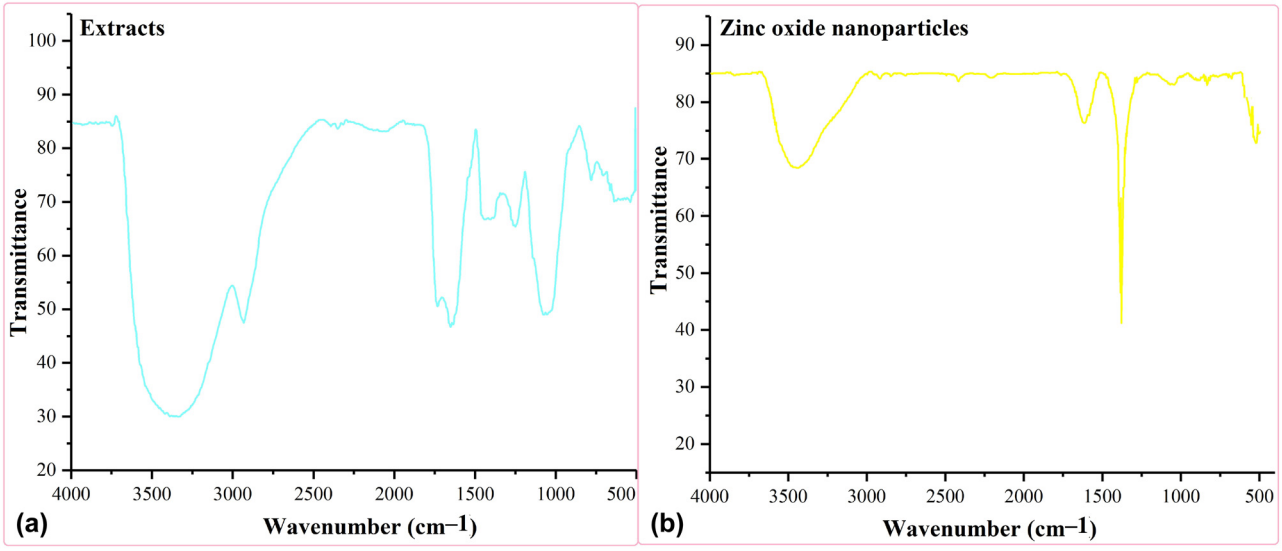

Figure 3: FTIR spectra of (a) extracts and (b) biosynthesized ZnONPs.

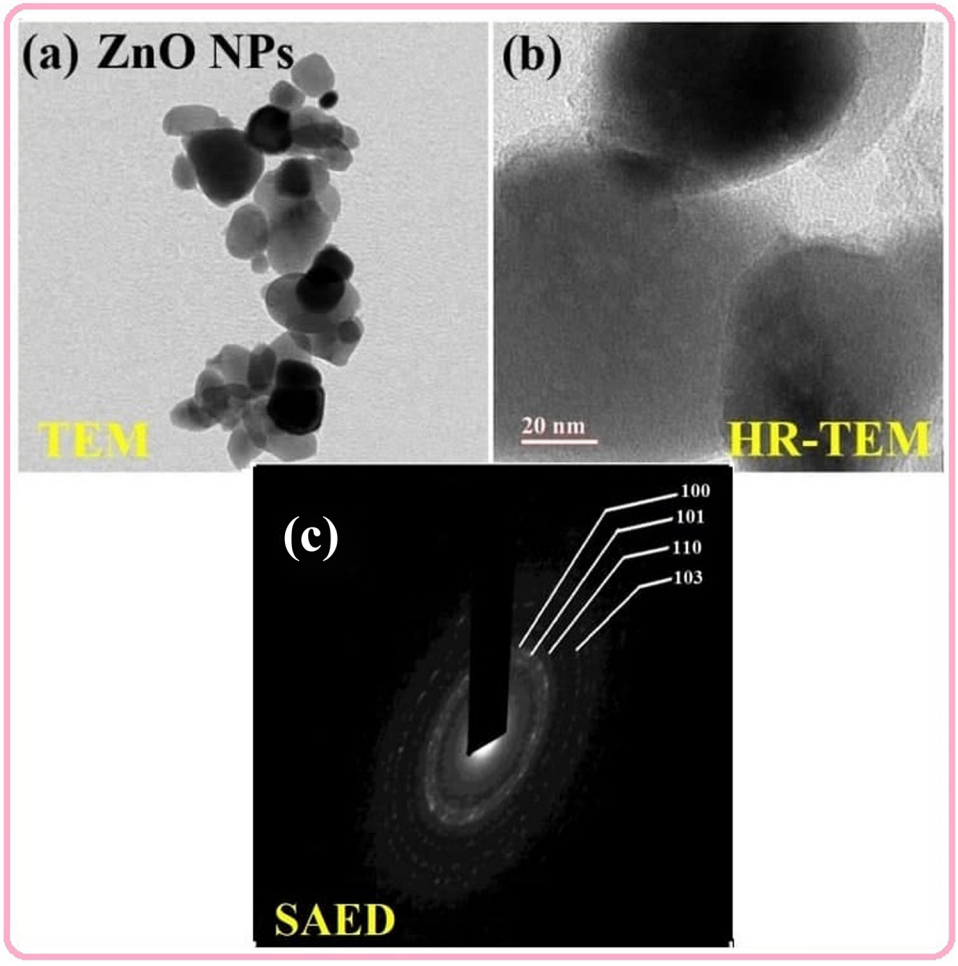

Figure 4: HRTEM analysis of ZnO NPs (a) showing that the NPs are spherical in high-resolution transmission electron microscopy (b) and the SAED pattern of the NP (c).

3.5 Antimicrobial potential of ZnO NPs

The identification of efficient antimicrobial agents from alternative sources has been motivated by the study of antibiotic-resistant pathogenic bacterial and fungus. However, only limited literatures support the effects of ZnO NPs on bacterial and fungal pathogens. The bactericidal activity of ZnO NP was assayed applying a disc diffusion technique against Gram-negative positive and positive bacterial strains such as *Escherichia coli* and *Bacillus subtilis* at concentration of 30 µg/mL of biogenic ZnO NPs. ZnONPs demonstrated significant antibacterial action against the strains tested when compared to the positive control based on the areas of inhibition. At a dose of 30 µg/mL, ZnONPs inhibited *B. subtilis* the most, followed by *E. coli*, with zones of inhibition of 23 and 15 mm, respectively, and antibacterial results were compared to standard reference; Cefepime (25 mm for *B. subtilis* and 23 mm inhibition zone for *E. coli*). Furthermore, the antibacterial activity of PCEs was evaluated, and it was discovered that the NP inhibited the growth of *B. subtilis* and *E. coli*, with inhibition zones of 13 and 12 mm, respectively, indicating that the NP demonstrated good antimicrobial activity when compared to extracts. The antibacterial efficiency of ZnONPs could be attributed to their smaller diameters, which is consistent with a finding indicating that ZnONPs with smaller diameters had powerful bactericidal effectiveness. In addition, the NP produced by the green technique using PCE were also found to be very active against the fungal species tested at a concentration of 50 µg/mL of manufactured ZnO NPs. The inhibition zones of *M. indicus* (19.5 mm), *H. insolens* (14.6 mm), and Clotrimazol (21.6 for *M. indicus* and 17.7 mm for *H. insolens*) clearly demonstrated that the fungal strains tested were sensitive to NP. PCEs also demonstrated antifungal activity, with inhibition zones of about 11 mm and 8 mm for *M. indicus* and *H. insolens*, respectively. As a result, the current study demonstrated that ZnO NP produced using PCE are a potential and effective antifungal agent against pathogenic fungal strains and are shown in Figure 5. As we all know, zinc oxide (ZnO) NP are being studied for production of next-generation nano-antibiotics against pathogenic bacteria in order to address multidrug resistance, a topic that has sparked substantial interest worldwide as a result of the use of nanotechnology. The size, particle size, crystallinity, and porosity of these ZnO NP (Figure 4 showing around 40–60 nm and has a sphere-like morphology) are all distinctive physicochemical characteristics. ZnO NPs demonstrate extensive antibacterial activity against a wide range of microorganisms, including Escherichia coli, Bacillus subtilis, and the

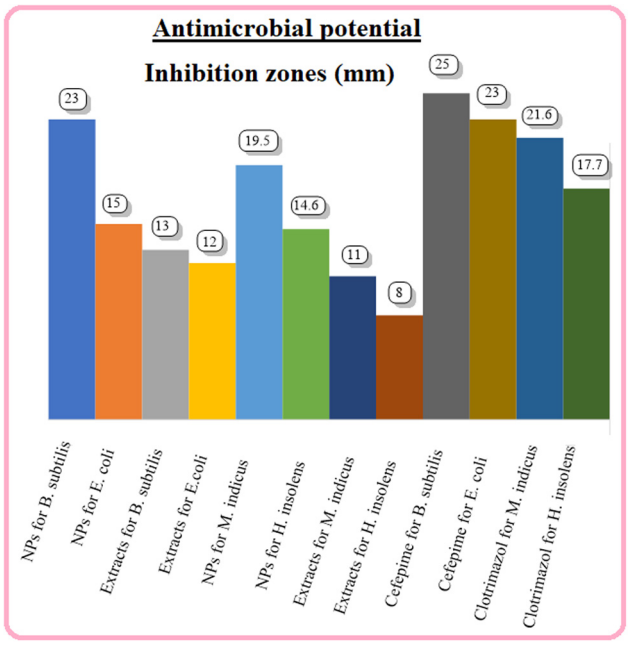

Figure 5: Antimicrobial activity of biogenic ZnO NP, extracts, and positive controls for bacterial and fungal strains.

M13 bacteriophage, based on these features [70,71]. As evidenced by assay data, the biogenic ZnO NPs exhibited strong antibacterial activities (Figure 5) due to increased specific surface area because of reduced particle size, resulting in higher particle surface reactivity. Furthermore, most microorganisms are in the hundreds of nanometers to tens of micrometers range, which can be destroyed either by contact of NP with cell walls or by entering the cells of microorganism. However, the mechanism of inhibitory effect of ZnO NPs on microbes is still unknown. Several studies have reported that incorporating ZnO NPs into bacterial cells causes continuous release of membrane lipids and proteins, altering bacterial cell membrane permeability and inhibiting microbes growth [72–74]. Despite its significant antimicrobial activity, ZnO NPs have high photooxidizing and photocatalysis activities, as well as high optical absorption in the UVA (315–400 nm) and UVB (280–315 nm) regions with biosafe materials that are beneficial in antimicrobial response and used as a UV protector in cosmetics [75].

3.6 *In vitro* biocompatibility and cytotoxicity effects analysis of NPs

A hemolytic activity assay using RBCs was performed to evaluate the biocompatibility of the biogenic NPs (RBCs). In this bioassay, hemolysis of RBCs was observed in response to varied ZnO NPs (25–400 g/mL). A

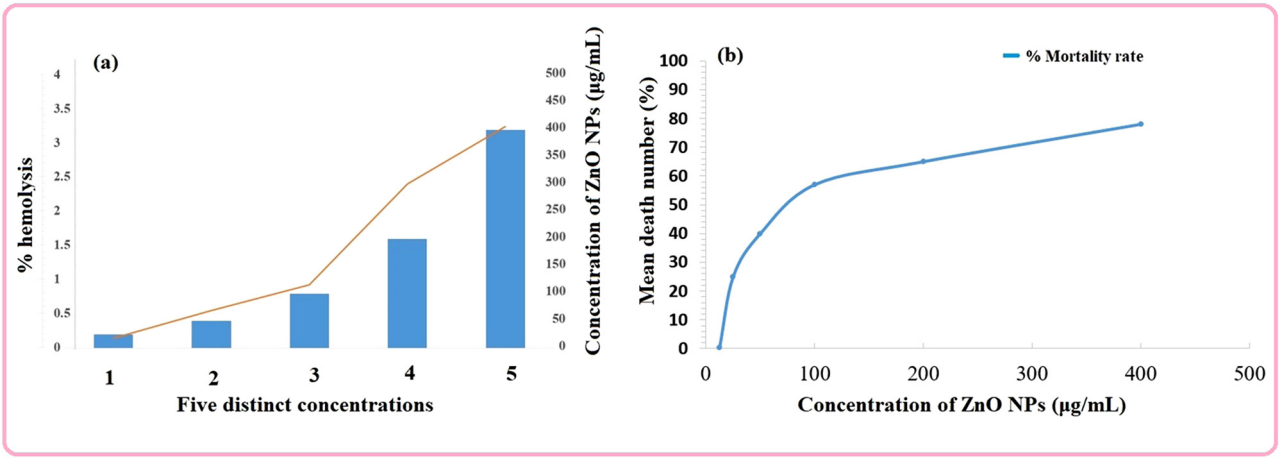

Figure 6: (a) % Hemolysis behavior of biogenic NPs at various concentrations and (b) correlation between NPs concentration and brine shrimp % mean mortality for cytotoxicity assessment.

spectrophotometer was used to measure the absorbance of RBCs at 570 nm to check for hemolysis. RBC hemolysis will be noticed only if the sample has the ability to rupture the cells. Only if the sample has the ability to rupture the cells will RBC hemolysis be detected. Figure 6a depicts the biocompatibility (hem-compatible) findings of ZnO NPs. According to the American Society for Testing Materials guidelines, biocompatibility of compounds with >2% hemolysis is designated as nonhemolytic, 2–5% slightly hemolytic, and >5% hemolytic [59]. Figure 6a suggests that different concentration doses of biosynthesized ZnO NPs demonstrate less hemolysis, even at 400 g/mL, confirming their high biocompatibility with erythrocytes as demonstrated in the literature [61]. The concentration dose of the biogenic ZnO NPs used in the biocompatibility test is several times higher than that of the amount employed for the antimicrobial activity test. The biocompatibility results of the study reveal that plant-based manufactured NP are biosafe, and ZnONPs would be used for clinical applications within certain concentration limits, as shown clearly in Figure 6a, where the percentage hemolysis of RBCs increases with increasing concentration of ZnO NPs.

Figure 6b shows dose-dependent trials in which the number of dead brine shrimp in experimental wells containing nanoparticle concentrations ranging from 12.5 to 400 µg/mL was counted after 24 h of exposure. The percentage of mortality was 0, 1, 25, 40, 57, 65, and 78% in concentration of 0 (without NP), 12.5, 25, 50, 100, 200, and 400 µg/mL of ZnO NPs, respectively. Based on experimental data, the highest mortality value of 78 ± 1.5 is observed at 400 µg/mL (found a graph with a similar pattern to that reported in the literature [61]), while the lowest value is found at 12.5 µg/mL (Figure 6b). The toxicity pattern of metallic NPs for *Artemia salina* is dose-dependent. Metallic NPs have a dose-dependent toxicity pattern for *Artemia salina*, according to experimental results. Toxicity of NPs can be caused by the NPs themselves, as well as their dissolution products and NP agglomerates formed during the experiment. Finally, using Organization for Economic Cooperation and Development (OECD) guidelines, NPs can be summarized and classified as low toxicity agents. Nonetheless, as indicated by cytotoxicity assay results, proper consideration should be given to the potential ecotoxicity and environmental health consequences of NPs.

3.7 Molecular docking analysis

A catalytic triad tunnel composed of Cys, His, and Asn is found in the active site of FabH (PDB: 1HNJ) (Figure 7a). The catalytic activity of an enzyme can be dramatically influenced, inhibited, or even stopped by affecting these amino acid residues [76]. Additionally, the active site residues of the FabH receptor are conserved across Gram-positive and Gram-negative bacteria, making FabH protein a promising therapeutic target for the development of innovative and broad-spectrum antimicrobial drugs as selective and nontoxic FabH inhibitors. To predict the *in vitro* efficiency of ZnO NPs (Figure 7b), the ligand-FabH model was used to perform molecular docking study. Docking of ZnO into a modeled receptor named beta-ketoacyl-acyl carrier protein synthase III (FabH) was done to investigate proper nanoparticle orientation within the receptor and obtain useful information for the active mechanism, including non-covalent interactions between the active site of the receptor and ZnONPs, which could lead to the development of new drugs for further biological research.

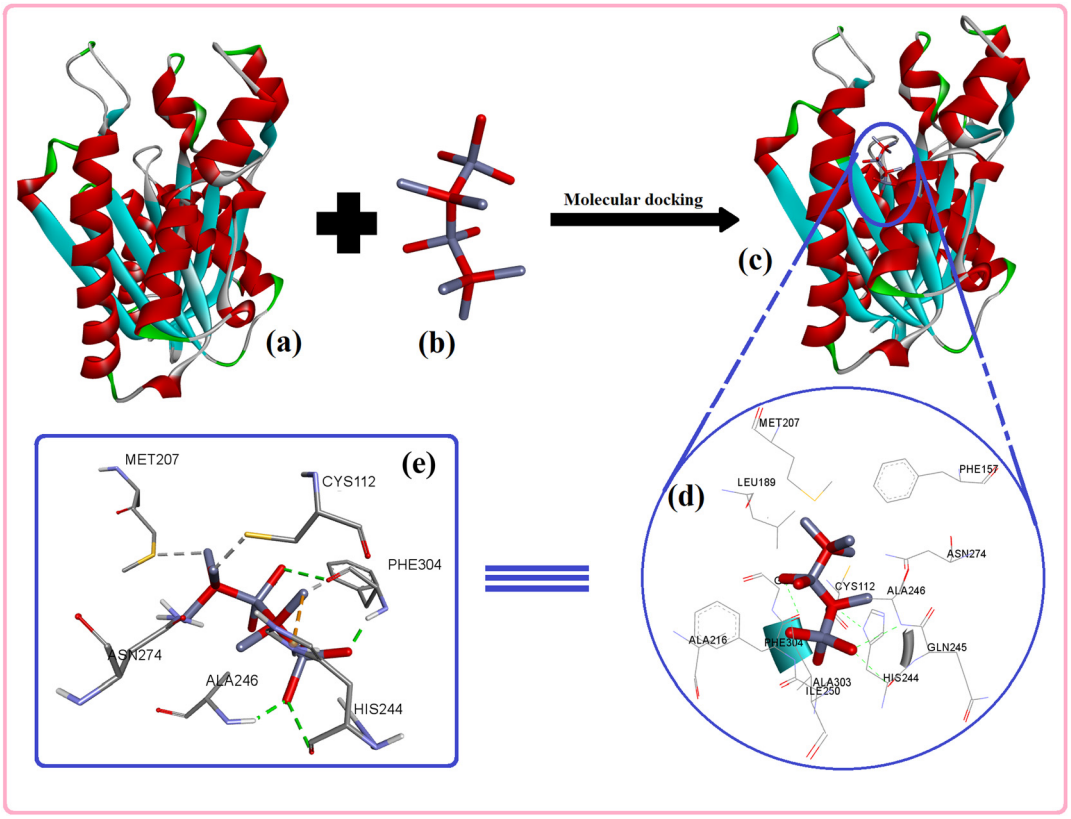

Figure 7: Molecular docking study of (a) receptor, (b) ligand (ZnO), (c) best docking pose and (d and e) various ZnO interactions with amino acids contribute to cavity formation.

The best docking posture selected based on the negative minimum energy (−6.79 kcal/mol) was considered as the best model to describe the interactions. Conventional hydrogen bonds were formed with 2.04857, 2.77139, and 2.90348 Å distances between the oxygen of ZnO NPs and the amino hydrogen of ALA246, PHE304, and HIS244, respectively (Figure 7c and d). Other non-covalent connections were formed between Zn of ZnONPs and CYS112:SG, MET207:SD, and PHE304:O, with distances of 2.43354, 3.2364, and 1.88611 Å, respectively, as well as a Pi–cation interaction between ZN0 and A:HIS244 with 2.87158 Å. The active amino acids cavity around ZnONPs is formed by residues like ALA303, ILE250, ALA216, GLN245, ASN274, PHE157, and LEU189. These interact weakly to keep ZnO in the proper orientation in the active pocket of the receptor, resulting in tight interactions between the ligand (ZnO) and the FabH receptor. Amino acid residues bind with ZnO NPs in docking experiments to stabilize the docked molecule in cavity, and the ligand can be thought of as a bacterial growth inhibitor in the living cell. Similarly, analogous interaction mechanisms may be employed to explain disturbances in the proliferation of fungal mycelium.

3.8 Photocatalytic activity

The rate of degradation of an organic dye pollutant (methylene blue [MB]) widely used in the dye industry was evaluated in a catalytic study under control experiments for photodegradation. The methylene blue dye solution was stirred with the catalyst in the dark to determine the adsorption loss, and the rate of degradation was calculated as the percentage of decolonization over time based on absorbance at the optimum wavelength of 664 nm as shown in Figure 8a.

The graph depicts the analysis of methylene blue decomposition by decreasing the peak intensities of the dye molecules over time. As shown in the diagram (Figure 8b), the degradation of the dye can be attributed to the generation of reactive oxygen species by the ZnO NPs in response to light irradiation. The generation of electron–hole pairs in ZnONPs, which are particularly active on the surface, is thought to be the mechanism of dye degradation in sunlight. The H_2O and O_2 molecules are oxidized by free holes and electrons traveling in the valence and conductance band bands, resulting in

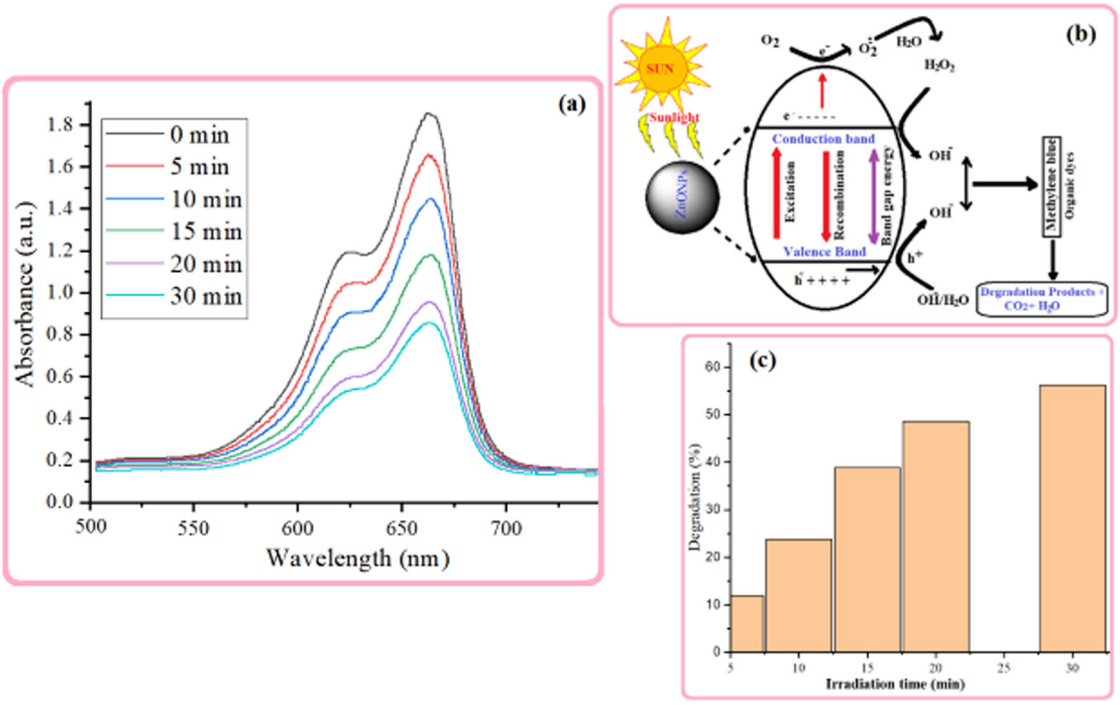

Figure 8: (a) Photocatalytic degradation of methylene blue using biogenic ZnO NPs, (b) photo trigger mechanism of ZnO NPs in dye degradation in direct sunlight and (c) degradation efficiency.

OH radicals and O_2^- ions, respectively; because of the blueshift and broad band gap of biogenic ZnO NPs, absorption of sunlight can easily increase the migration of electrons and the positive hole, resulting in increased degradation efficiency, as depicted in a schematic diagram (Figure 8a–c).

4 Conclusion

Biogenic ZnONPs were well-synthesized in an environmentally friendly way using extracts of pine cone obtained from Korean red pine (*Pinus densiflora*), and their physical, chemical, and morphological properties were confirmed using UV-Vis, FTIR, XRD, HRTEM, and SAED with particle sizes ranging from 40 to 60 nm. The photocatalytic activity of the produced NP against methylene blue dye was remarkable, with a maximum of 60% degradation recorded in a short period of time under sunlight irradiation. Furthermore, when compared to extracts, ZnONPs exhibit good bactericidal activity and antifungal activity, but less than reference drugs against pathogenic Gram-negative *E. coli* and Gram-positive *B. subtilis* bacterial strains, as well as two human pathogenic fungi, *H. insolens* and *M. indications*, respectively. As a result, ZnO NPs can be employed as an antibacterial in pharmaceuticals, cosmetics, ointments, lotions, and among other applications. A molecular docking was also performed to investigate the binding interactions between NP and receptors. It may be concluded that ZnO NP are an effective antimicrobial agent against pathogenic microorganisms, and interactions between receptors and ZnONPs will allow researchers to gain a grasp of the molecular method for producing non-toxic germ inhibitors. In brief, the findings suggested that NP could be promising materials for the degradation of visible light dyes as well as antibacterial agents.

Funding information: The author states no funding involved.

Author contributions: The author has accepted responsibility for the entire content of this manuscript and approved its submission.

Conflict of interest: The author states no conflict of interest.

References

[1] Albrecht MA, Evans CW, Raston CL. Green chemistry and the health implications of nanoparticles. Green Chem. 2006;8:417–32.
[2] Arangasamy L, Munusamy V. Tapping the unexploited plant resources for the synthesis of silver nanoparticles. Afr J Biotechnol. 2008;7:3162–5.

[3] Yadav T, Mungray AA, Mungray AK. Fabricated nanoparticles. Rev Env Contam Toxicol. 2014;230:83–110.
[4] Research BCC. Glob mark nanocomposites, nanoparticles, nanoclays, nanotubes. 2014. https://www.bccresearch.com/market-research/nanotechnology.
[5] Srivastav AK, Kumar M, Ansari NG, Jain AK, Shankar J, Arjaria N, et al. A comprehensive toxicity study of zinc oxide nanoparticles versus their bulk in wistar rats: toxicity study of zinc oxide nanoparticles. Hum Exp Toxicol. 2016;35(12):1286–304.
[6] Ghosh M, Jana A, Sinha S, Jothiramajayam M, Nag A, Chakraborty A, et al. Effects of ZnO nanoparticles in plants: cytotoxicity, genotoxicity, deregulation of antioxidant defenses, and cell-cycle arrest. Mutat Res Genet Toxicol Env Mutagen. 2016;807:25–32.
[7] Sabir S, Arshad M, Chaudhari SK. Zinc oxide nanoparticles for revolutionizing agriculture: synthesis and applications. Sci World J. 2014;2014(8):925494–8.
[8] Mousa A, Alghuthaymi MA, Almoammar H, Rai M, Said-Galiev E, Abd-Elsalam KA. Myconanoparticles: synthesis and their role in phytopathogens management. Biotechnol Biotechnol Equip. 2015;29:221–36.
[9] Alexander J. History of the medical use of silver. Surg Infect. 2009;10:289–92.
[10] Yasuyuki M, Kunihiro K, Kurissery S, Kanavillil N, Sato Y, Kikuchi Y. Antibacterial properties of nine pure metals: a laboratory study using Staphylococcus aureus and Escherichia coli. Biofouling. 2010;26:851–8.
[11] Lemire JA, Harrison JJ, Turner RJ. Antimicrobial activity of metals: mechanisms, molecular targets, and applications. Nat Rev Microbiol. 2013;11:371–84.
[12] Turner R. Metal-based antimicrobial strategies. Microb Biotechnol. 2017;10:1062–5.
[13] Stadtman E. Oxidation of free amino acids and amino acid residues in proteins by radiolysis and by metal-catalyzed reactions. Annu Rev Biochem. 1993;62:797–821.
[14] Stadtman ER, Levine RL. Free radical-mediated oxidation of free amino acids and amino acid residues in proteins. Amino Acids. 2003;25:207–18.
[15] Valko M, Morris H, Cronin MT. Metals, toxicity and oxidative stress. Curr Med Chem. 2005;12:1161–208.
[16] Li WR, Xie XB, Shi QS, Zeng HY, Ou-Yang YS, Chen YB. Antibacterial activity and mechanism of silver nanoparticles on Escherichia coli. Appl Microbiol Biotechnol. 2009;85:1115–22.
[17] Pereira Y, Lagniel G, Godat E, Baudouin-Cornu P, Junot C, Labarre J. Chromate causes sulfur starvation in yeast. Toxicol Sci. 2008;106:400–12.
[18] Nishioka H. Mutagenic activities of metal compounds in bacteria. Mutat Res. 1975;31:185–9.
[19] Green MH, Muriel WJ, Bridges BA. Use of a simplified fluctuation test to detect low levels of mutagens. Mutat Res. 1976;38:33–42.
[20] Wong P. Mutagenicity of heavy metals. Bull Env Contam Toxicol. 1988;40(4):597–603.
[21] Shah M, Fawcett D, Sharma S, Tripathy SK, Poinern GEJ. Green synthesis of metallic nanoparticles via biological entities. Materials. 2015;8(11):7278–308.
[22] Yang Y, Serrano LA, Guldin SA. Versatile AuNP Synthetic platform for decoupled control of size and surface composition. Langmuir. 2018;34:6820–6.
[23] Iarossi M, Schiattarella C, Rea I, Stefano LD, Fittipaldi R, Vecchione A, et al. colorimetric immunosensor by aggregation of photochemically functionalized gold nanoparticles. ACS Omega. 2018;3:3805–12.
[24] Bansal K, Aqdas M, Kumar M, Bala R, Singh S, Agrewala JN, et al. A facile approach for synthesis and intracellular delivery of size tunable cationic peptide functionalized gold nanohybrids in cancer cells. Bioconjugate Chem. 2018;29:1102–10.
[25] Gutiérrez JA, Caballero S, Díaz LA, Guerrero MA, Ruiz J, Ortiz CC. High antifungal activity against candida species of monometallic and bimetallic nanoparticles synthesized in nanoreactors. ACS Biomater Sci Eng. 2018;4:647–53.
[26] Elina H, Hana W, Shlomi P, Hadas S, David Z, Orit S. meso-Tetrahydroxyphenylchlorin-conjugated gold nanoparticles as a tool to improve photodynamic therapy. ACS Appl Mater Interfaces. 2018;10:2319–27.
[27] Urawadee R, Vijayalekshmi S. Recent developments in antimicrobial-peptide-conjugated gold nanoparticles. Bioconjugate Chem. 2017;28:2673–86.
[28] Adabi M, Naghibzadeh M, Adabi M, Zarrinfard MA, Esnaashari S, Seifalian AM, et al. Biocompatibility and nanostructured materials: applications in nanomedicine. Artif Cell Nanomed Biotechnol. 2017;45:833–42.
[29] Gautama A, van Veggel FCJM. Synthesis of nanoparticles, their biocompatibility, and toxicity behavior for biomedical applications. J Mater Chem B. 2013;1:5186–200.
[30] Li X, Wang L, Fan Y, Feng Q, Cui F-Z. Biocompatibility and toxicity of nanoparticles and nanotubes. J Nanomater. 2012;2012:548389.
[31] Mahendra C, Murali M, Manasa G, Ponnamma P, Abhilash M, Lakshmeesha T, et al. Antibacterial and antimitotic potential of bio-fabricated zinc oxide nanoparticles of Cochlospermum religiosum (L.). Microb Pathog. 2017;110:620–9.
[32] Sukri S, Shameli K, Wong MM-T, Teow S-Y, Chew J, Ismail NA. Cytotoxicity and antibacterial activities of plant-mediated synthesized zinc oxide (ZnO) nanoparticles using Punica granatum (pomegranate) fruit peels extract. J Mol Struct. 2019;1189:57–65.
[33] Brigger I, Dubernet C, Couvreur P. Nanoparticles in cancer therapy and diagnosis. Adv Drug Deliv Rev. 2002;54:631–51.
[34] Mandal D, Bolander ME, Mukhopadhyay D, Sankar S, Mukherjee P. The use of microorganisms for the formation of metal nanoparticles and their application. Appl Microbiol Biotechnol. 2006;69(5):485–92.
[35] Danhong Y, Guangfu Y, Zhongbing, Liang L, Xiaoming L, Xianchun C, et al. Cellular compatibility of biomineralized ZnO nanoparticles based on prokaryotic and eukaryotic systems. Langmuir. 2011;27:13206–11.
[36] Nikolova MP, Chavali MS. Metal oxide nanoparticles as biomedical materials. Biomimetics. 2020;5(2):27.
[37] Busi S, Rajkumari J. Microbially synthesized nanoparticles as next generation antimicrobials: scope and applications. In: Grumezescu AM, editor. Nanoparticles in pharmacotherapy. Norwich, NY: Elsevier; 2019. p. 485–524.
[38] Ghosh S, Ahmad R, Zeyaullah M, Khare SK. Microbial nanofactories: synthesis and biomedical applications. Front Chem. 2021;9:626834.
[39] Attarad A, Abdul-Rehman P, Muhammad Z. Elemental zinc to zinc nanoparticles: is ZnO NPs crucial for life? Synthesis,

toxicological, and environmental concerns. Nanotechnol Rev. 2018;7(5):413–41.
[40] Moezzi A, McDonagh AM, Cortie MB. Zinc oxide particles: synthesis, properties and applications. Chem Eng J. 2012;185:1–22.
[41] Nair S, Sasidharan A, Rani VD, Menon D, Nair S, Manzoor K, et al. Role of size scale of ZnO nanoparticles and microparticles on toxicity toward bacteria and osteoblast cancer cells. J Mater Sci Mater Med. 2009;20:235–41.
[42] Lu H, Wang J, Stoller M, Wang T, Bao Y, Hao H. An overview of nanomaterials for water and wastewater treatment. Adv Mater Sci Eng. 2016;2016:4964828.
[43] Kyung HJ, In SH, Ji EK, Young JL, Moon HK, Young HL, et al. Antibacterial effects of aqueous extract purified from the immature cone of red pine (Pinus densiflora). Text Color Finish. 2014;26:45–52.
[44] Chung SK, Sung CM, Mee SL. Antioxidant, antimutagenic, and antitumor effects of pine needles (Pinus densiflora). Nutr Cancer. 2006;56(2):162–71.
[45] Jung MJ, Chung HY, Choi JH, Choi JS. Antioxidant principals from the needles of red pine, Pinus densiflora. Phytother Res. 2003;17(19):1064–8.
[46] Lim UK, Yoo JJ, Lee JY. Pine needles. Health Care with Pine Needles. Seoul, Korea: Jin Myung; 1993. p. 52–83
[47] Jieun C, Woong K, Jaeyoung P, Hyeonsook C. The beneficial effects of extract of pinus densiflora needles on skin health. Microbiol Biotechnol Lett. 2016;44:208–17.
[48] Seung-Hyun L, Tae-Won J, Ji-Soo C, Jeong-Yun M, Jae-Ho P. Inhibitory Effects of pine cone (*Pinus densiflora*) on melanogenesis in B16F10 melanoma cells. Korean J Plant Res. 2019;32:275–81.
[49] Velmurugan P, JPark JH, Lee SM, Jang JS, Lee KJ, Han SS, et al. Synthesis and characterization of nanosilver with antibacterial properties using Pinus densiflora young cone extract. J Photochem Photobiol B Biol. 2015;147:63–8.
[50] Velmurugan P, JPark JH, Lee SM, Jang JS, Lee KJ, Han SS, et al. Phytofabrication of bioinspired zinc oxide nanocrystals for biomedical application. Artif Cell Nanomed B. 2016;44(6):1529–36.
[51] Singh N, Haque FZ. Synthesis of zinc oxide nanoparticles with different pH by aqueous solution growth technique. Optik. 2016;127:174–7.
[52] Varadavenkatesan T, Lyubchik E, Pai S, Pugazhendhi A, Vinayagam R, Selvaraj R. Photocatalytic degradation of Rhodamine B by zinc oxide nanoparticles synthesized using the leaf extract of Cyanometra ramiflora. J Photochem Photobiol B. 2019;199:111621.
[53] Brindhadevi K, Samuel MS, Verma TN, Vasantharaj S, Sathiyavimal S, Saravanan M, et al. Zinc oxide nanoparticles (ZnONPs)-induced antioxidants and photocatalytic degradation activity from hybrid grape pulp extract (HGPE). Biocatal Agric Biotechnol. 2020;28:101730.
[54] Bing H, Jin Z, Xiu-Min W. Decoloring methyl orange under sunlight by a photocatalytic membrane reactor based on ZnO nanoparticles and polypropylene macroporous membrane. Int J Polym Sci. 2013;2013(451398):1–8.
[55] Clinical and Laboratory Standards Institute (CLSI). Methods for antimicrobial dilution and disk susceptibility testing of infrequently isolated or fastidious bacteria. 3rd edn. CLSI document; 2016. p. M45
[56] Vishvanath T, Neha M, Keval G, Solanki PS, Shah NA, Monalisa T. Mechanism of anti-bacterial activity of zinc oxide nanoparticle against carbapenem-resistant acinetobacter baumannii. Front Microbiol. 2018;9(1218):1–9.
[57] Li X, Robinson SM, Gupta A, Saha K, Jiang Z, Moyano DF, et al. Functional gold nanoparticles as potent antimicrobial agents against multi-drug-resistant bacteria. ACS Nano. 2014;8(10):10682–86.
[58] Sarker SR, Polash SA, Boath J, Kandjani AE, Poddar A, Dekiwadia C, et al. Functionalization of elongated tetrahexahedral au nanoparticles and their antimicrobial activity assay. ACS Appl Mater Interfaces. 2019;11:13450–59.
[59] Nasar MQ, Khalil AT, Ali M, Shah M, Ayaz M, Shinwari ZK. Phytochemical analysis, ephedra procera C. A. Mey. Mediated green synthesis of silver nanoparticles, their cytotoxic and antimicrobial potentials. Medicina. 2019;55(369):17.
[60] Alam M, Alam MJ, Nami SAA, Khan MS, Ahmad S, Lee D. UDFT, Hirshfeld surfaces, spectral and *in vivo* cytotoxic studies of 7a-Aza-B-homostigmast-5-eno [7a,7-d] tetrazole. J Mol Struct. 2015;1099:588–600.
[61] Faisal S, Jan H, Shah SA, Shah S, Khan A, Akbar MT, et al. Green synthesis of zinc oxide (ZnO) nanoparticles using aqueous fruit extracts of myristica fragrans: their characterizations and biological and environmental applications. ACS Omega. 2021;6:9709–22.
[62] Arulvasu C, Jennifer SM, Prabhu D, Chandhirasekar D. Toxicity effect of silver nanoparticles in brine shrimp *Artemia*. Sci World J. 2014;2014(256919):10.
[63] Morris GM, Huey R, Lindstrom W, Sanner MF, Belew RK, Goodsell DS, et al. Autodock4 and AutoDockTools4: automated docking with selective receptor flexiblity. J Comput Chem. 2009;30:2785–91.
[64] Biovia DS. Discovery studio modeling environment. San Diego: Dassault Systemes, Release 4; 2015.
[65] Chung HJ, Hwang GH, Yoo MJ, Rhee SJ. Chemical composition of pine sprouts and pine needles for the production of pine sprout tea. J Korean Soc Food Cult. 1996;11(5):635–41.
[66] Singh J, Kaur S, Kaur G, Basu S, Rawat M. Biogenic ZnO nanoparticles: a study of blueshift of optical band gap and photocatalytic degradation of reactive yellow dye under direct sunlight. Green Process Synth. 2019;8:272–80.
[67] Del Buono D, Di Michele A, Costantino F, Trevisan M, Lucini L. Biogenic ZnO nanoparticles synthesized using a novel plant extract: application to enhance physiological and biochemical traits in maize. Nanomaterials. 2021;11(5):1270.
[68] Rajashekara S, Shrivastava A, Sumhitha S, Kumari S. Biomedical applications of biogenic zinc oxide nanoparticles manufactured from leaf extracts of calotropis gigantea (L.) dryand. BioNanoScience. 2020;10:654–71.
[69] Chengwu Y, Christof W. IR spectroscopy applied to metal oxide surfaces: adsorbate vibrations and beyond. Adv Phys X. 2017;2:373–408.
[70] Sirelkhatim A, Mahmud S, Seeni A, Kaus NHM, Ann LC, Bakhori SKM, et al. Review on zinc oxide nanoparticles: antibacterial activity and toxicity mechanism. Nanomicro Lett. 2015;7(3):219–42.
[71] Jin S-E, Hyo-Eon J. Antimicrobial activity of zinc oxide nano/microparticles and their combinations against pathogenic

microorganisms for biomedical applications: from physico-chemical characteristics to pharmacological aspects. Nanomaterials. 2021;11:263–98.
[72] Amro NA, Kotra LP, Wadu-Mesthrige K, Bulychev A, Mobashery S, Liu G. High-resolution atomic force microscopy studies of the Escherichia coli outer membrane: structural basis for permeability. Langmuir. 2000;16:2789–96.
[73] Brayner R, Ferrari-Iliou R, Brivois N, Djediat S, Benedetti MF, Fievet F. Toxicological impact studies based on Escherichia coli bacteria in ultrafine ZnO nanoparticles colloidal medium. Nano Lett. 2006;6:866–70.
[74] Song Z, Kelf TA, Sanchez WH, Roberts MS, Rička J, Frenz M, et al. Characterization of optical properties of ZnO nanoparticles for quantitative imaging of transdermal transport. Biomed Opt Exp. 2011;2(12):3321–33.
[75] Gudkov SV, Burmistrov DE, Serov DA, Rebezov MB, Semenova AA, Lisitsyn AB. A mini review of antibacterial properties of ZnO nanoparticles. Front Phys. 2021;9:641481.
[76] Davies C, Heath RJ, White SW, Rock CO. The 1.8 Å crystal structure and active-site architecture of β-ketoacyl-acyl carrier protein synthase III (FabH) from Escherichia coli. Structure. 2000;8:185–95.